ACS Photonics

Letter

pubs.acs.org/journal/apchd5

Observation of Magnetoplasmons in Bi_2Se_3 Topological Insulator

Marta Autore,[†] Hans Engelkamp,[‡] Fausto D'Apuzzo,[§] Alessandra Di Gaspare,[∥] Paola Di Pietro,[⊥] Irene Lo Vecchio,[#] Matthew Brahlek,[○] Nikesh Koirala,[○] Seongshik Oh,[○] and Stefano Lupi*[,†]

[†]INFN and Dipartimento di Fisica, [§]Istituto Italiano di Tecnologia and Dipartimento di Fisica, and [#]Dipartimento di Fisica, Università di Roma "La Sapienza", Piazzale A. Moro 2, I-00185 Roma, Italy

[‡]High Field Magnet Laboratory, Institute for Molecules and Materials, Radboud University Nijmegen, Toernooiveld 7, NL-6525 ED Nijmegen, The Netherlands

[∥]LNF-INFN and CNR-IFN, Via E. Fermi 40, 00044 Frascati, Italy

[⊥]INSTM Udr Trieste-ST and Sincrotrone Trieste, Area Science Park, I-34012 Trieste, Italy

[○]Department of Physics and Astronomy Rutgers, The State University of New Jersey 136 Frelinghuysen Road Piscataway, New Jersey 08854-8019, United States

S *Supporting Information*

ABSTRACT: Both the collective (plasmon) and the single particle (Drude) excitations of an electron gas can be controlled and modified by an external magnetic field B. At finite B, plasmon gives rise to a magnetoplasmon mode and the Drude term to a cyclotron resonance. These magnetic effects are expected to be extremely strong for Dirac electrons with a linear energy-momentum dispersion, like those present in graphene and topological insulators (TIs). Here, we investigate both the plasmon and the Drude response versus B in Bi_2Se_3 topological insulator. At low B, the cyclotron resonance is still well separated in energy from the magnetoplasmon mode; meanwhile, both excitations asymptotically converge at the same energy for increasing B, consistently with a dynamical mass for Dirac carriers of $m_D^* = 0.18 \pm 0.01\ m_e$. In TIs, one then achieves an excellent magnetic control of plasmonic excitations and this could open the way toward plasmon controlled terahertz magneto-optics.

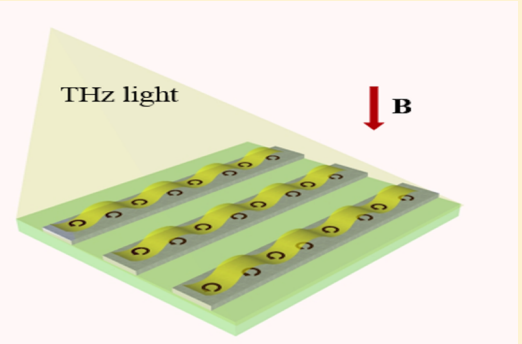

KEYWORDS: *topological insulators, plasmons, cyclotron resonance, Dirac carriers, dynamical mass*

Topological insulators (TIs) are novel quantum materials with insulating electronic states in the bulk and metallic states at their surface and edge. This intrinsically stratified electronic distribution is due to a band inversion occurring because of the strong spin−orbit coupling in these materials, which leads to nontrivial topological invariants.[1−3] The surface metallic states of a TI show many exotic features, such as chiral spin texture, backscattering protection due to time-reversal symmetry, and Dirac-like linear energy-momentum dispersion. Furthermore, unlike graphene, TI surface states spontaneously provide a 2D Dirac-Fermion system segregated from the bulk material without the need of physically implementing an atomic monolayer. Because of these peculiar features, TIs are very suitable for novel applications like quantum computing,[4,5] THz detectors,[6] spintronic devices,[7] and plasmonics.[8,9]

Among TIs, Bi_2Se_3 is one of the most promising materials because of the large bulk gap $E_g \simeq 300$ meV. Recently, it has been shown that both transport[10] and low-energy single-particle[11] and collective (plasmon)[8] electrodynamics response are dominated by surface Dirac electrons in Bi_2Se_3 thin films with thickness $d < 300$ quintuple layers (1 QL $\simeq$ 1 nm). However, the possible contribution to those propertied from an accumulation layer of 2D massive electron at the surface of Bi_2Se_3 due to a band-bending effect, has been suggested in ref 12.

A challenging issue concerning plasmonics is modulation of the propagating and localized plasmon excitations via external parameters such as electrostatic gating,[13] optical pulses,[14] or magnetic field.[15] The modulation of plasmons via magnetic field, a branch called magnetoplasmonics, is particularly interesting, because enhanced magneto-optical effects are expected to appear in correspondence with plasmonic excitations.[15,16] These effects have been recently demonstrated in graphene[17] and should be even stronger in the case of chirally textured TI surface states.[18]

Despite the extreme interest in investigating the properties of Dirac plasmons in topological insulators under a strong magnetic field, no measurement was reported so far. In this paper we fill this gap by investigating the behavior of Dirac plasmons under a strong magnetic field in Bi_2Se_3. In particular, we studied the plasmon (collective) excitation in an array of microribbons for terahertz light perpendicularly polarized to

Received: January 29, 2015
Published: August 20, 2015

DOI: 10.1021/acsphotonics.5b00036
ACS Photonics 2015, 2, 1231−1235

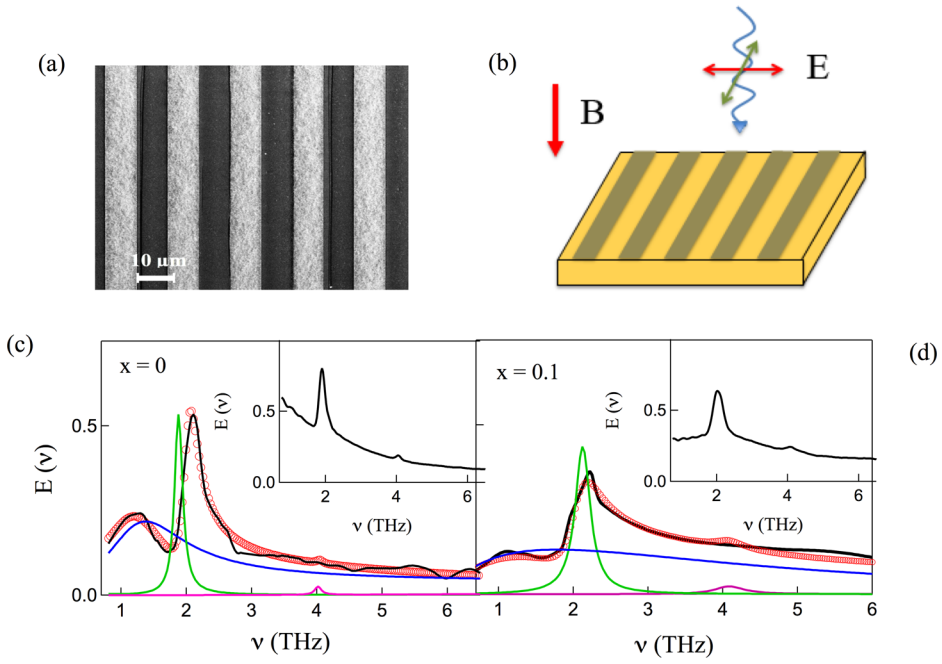

Figure 1. (a) SEM picture of the patterned $x = 0$ film. (b) Sketch of the magneto-optic measurement configuration. (c, d) Zero field extinction spectra for $(Bi_{1-x}In_x)_2Se_3$ ($x = 0$, 0.1), ribbon arrays with light polarized perpendicular to the ribbons (extinction spectra for the unpatterned samples in the inset). Fano fit (red empty circles) accounting for plasmon−phonon interaction (see Supporting Information) at 1.6 K. The bare plasmon curve is represented as a solid blue line, while the α (β)-phonon is represented as a green (purple) solid curve.

ribbons at 1.6 K and for a magnetic field B from 0 to 30 T. The plasmon evolution with B has been further compared to the Drude (single-particle) term as observed with linearly polarized light along the ribbons, in the same experimental conditions.

Already at low-fields, the Drude term evolves into a cyclotron resonance (CR) at finite energy which, however, is still well separated from the magnetoplasmon mode. For increasing B they merge together, giving rise to a unique Dirac magnetic excitation onto the surface of Bi_2Se_3. The evolution with B of both cyclotron resonance and magnetoplasmon provides two independent estimates of the dynamical mass of Dirac carriers which results in both cases $m^*_D = 0.18 \pm 0.01$ m_e.

A similar experiment has been performed on $(Bi_{0.9}In_{0.1})_2Se_3$, a compound, which shows a trivial insulating phase, achieved from the topological phase of Bi_2Se_3 by a quantum phase transition (QPT) through In substitution in Bi sites.[19,20] This system has the same crystal structure of Bi_2Se_3 and is characterized by massive (Schrödinger) electrons (having a quadratic energy/momentum dispersion), with a similar surface density to Bi_2Se_3.[19] At variance with the Dirac plasmon in Bi_2Se_3, in this case, the plasmon mode is strongly overdamped, suggesting that the topological protection of Dirac electrons plays a fundamental role in the plasmon lifetime. Moreover, the magnetic behavior of the Schrödinger plasmon is consistent with a cyclotron mass $m^*_S = 0.12$ m_e in good agreement with results obtained by photoemission spectroscopy.[19,21]

In TIs, where single-particle and collective electronic response are determined by Dirac electrons, one then achieves an excellent magnetic control of plasmonic excitations. This could pave the way toward strong magneto-optical effects and Dirac plasmon controlled terahertz magneto-optics.

RESULTS AND DISCUSSION

High quality thin films of $(Bi_{1-x}In_x)_2Se_3$ were fabricated through molecular beam epitaxy (MBE),[10,22] with a thickness of 60 QL, on 10×10 mm^2 Al_2O_3 substrate. Indium substitution was set to $x = 0$ (with a Dirac electron surface density $n_D = 3 \pm 1 \times 10^{13}$ cm^{-2}), and $x = 0.1$ (massive electron surface density $n_S = 2.5 \pm 1 \times 10^{13}$ cm^{-2}), thus, covering both the topological and the trivial phases, respectively.[19,20]

High magnetic field terahertz transmittance $T(\nu)$ measurements of $(Bi_{1-x}In_x)_2Se_3$ ($x = 0$; 0.1) as-grown and patterned films with respect the bare Al_2O_3 substrate have been performed at the High Field Magnet Laboratory in Nijmegen (The Netherlands) using a Bruker IFS113v spectrometer coupled to a resistivity magnet. Light propagated (Figure 1b) parallel to the magnetic field direction and perpendicular to the sample surface (Faraday geometry). The temperature was set at 1.6 K and the field was varied from 0 to 30 T, with 2.5 T steps.

Zero Field THz Data. Extinction coefficient $E(\nu) = 1 - T(\nu)$ at $T = 1.6$ K for the as-grown films are shown in the inset of Figure 1c,d. Curves show both the α- and β-phonon modes at nearly 1.85 and 4.0 THz, respectively, characteristic of Bi_2Se_3 bulk,[23] which undergo a slight broadening for x(In) = 0.1 film. Phonons are superimposed to a Drude-like free carrier contribution. As shown in ref 11, in pure Bi_2Se_3 films, both the Drude and the plasmon response at low-T are mainly due to Dirac carriers (see also SI); meanwhile, for the $x = 0.1$ film, the terahertz response is determined only by massive surface electrons.[19] The Drude scattering rate changes from 1.4 THz for the undoped Bi_2Se_3 film to about 5 THz for the $x = 0.1$ doped one, as already reported by Wu et al.,[20] and therein associated with the loss of topological protection of surface carriers.

A micropatterning of the sample breaks the translational symmetry, thus, providing the extra wavevector necessary for the light absorption. This condition allows to excite plasmons,[13] providing information about the collective charge-carrier behavior across the quantum-phase transition. All samples have been patterned through electron beam lithography (EBL)

DOI: 10.1021/acsphotonics.5b00036
ACS Photonics 2015, 2, 1231−1235

and reactive ion-etching at CNR-IFN in Rome, in the form of microribbon arrays of width W = 8 μm and period 2W. A scanning electron microscopy (SEM) picture is displayed in Figure 1a for the x = 0 sample.

Figure 1c (Figure 1d) shows the extinction spectrum of Bi_2Se_3 ($(Bi_{0.9}In_{0.1})_2Se_3$) for incident light perpendicularly polarized to the ribbons. In this case, a plasmon is excited, with momentum $q \sim \pi/W$. The interference between the plasmon and the α-phonon generates an asymmetric extinction profile, which can be modeled via the Fano theory[24] (see Supporting Information). Following the procedure used by Di Pietro et al.[8] and using values extracted from the as-grown films for the phonon parameters, we were able to fit the mixed plasmon−phonon profile to extract the bare line shapes of the two modes, as shown in Figure 1c,d. While the α- (green) and β-phonons (purple) slightly broaden with increasing In content, as in the as-grown film case, the plasmon mode (blue) undergoes a strong broadening through the topological transition. The fitting procedure allows us to extract quantitative values for the plasmon scattering rate Γ_{pl}. The values obtained are Γ_{pl} = 1.45 THz (x = 0) and Γ_{pl} = 4.95 THz (x = 0.1). These values perfectly coincide with those of the Drude term, as measured both in unpatterned films coming from the same batch and in patterned films for light polarization parallel to the ribbons (see above). This means that the plasmon lifetime is mainly determined by ohmic loss (the electromagnetic losses start to be effective at lower transversal size of ribbons[8]) and through the QPT one transforms topologically protected plasmons, that is, based on Dirac electrons, in trivial ones, related to massive carriers. Conversely, this experimental result suggests that the nature of electrons, Dirac topologically protected charge carriers in Bi_2Se_3, and massive nontopologically protected charge-carriers in ($(Bi_{0.9}In_{0.1})_2Se_3$), could be traced across the QPT through the behavior of their collective plasmon modes.

Magnetoplasmons. In order to better investigate the nature of the plasmonic excitations in the topological (x = 0) and trivial (x = 0.1) phase, we study the extinction spectra under the application of a high magnetic field. In this case, a mixing between the plasmon and cyclotron excitations takes place giving rise to the combined mode, called magnetoplasmon, whose characteristic frequency ν_{mp}, as established in a long series of experiments, follows the equation[25]

$$\nu_{mp} = \sqrt{\nu_{pl}^2 + \nu_c^2} \tag{1}$$

where ν_{pl} is the plasmon frequency at zero field and ν_c is the cyclotron frequency for the surface carriers. As in our sample, the Fermi energy is $E_F \simeq 400$ meV, well above the Dirac point, the cyclotron resonance takes the following classical dependence on the magnetic field

$$\nu_c = \frac{eB}{2\pi m^*} \tag{2}$$

where m^* is the dynamical mass given by $m^* = \frac{E_F}{v_F^2}$, v_F being the Fermi velocity.[26] The effect of the hybridization between the cyclotron resonance and the plasmon mode is shown in Figure 2a, where the extinction spectra for the topological phase in Bi_2Se_3 are displayed for a magnetic field ranging from 0 to 30 T.

In this figure, one can clearly see that, at low-fields, the magnetoplasmon still interacts with the α-phonon mode determining a Fano shape in the extinction coefficient, already

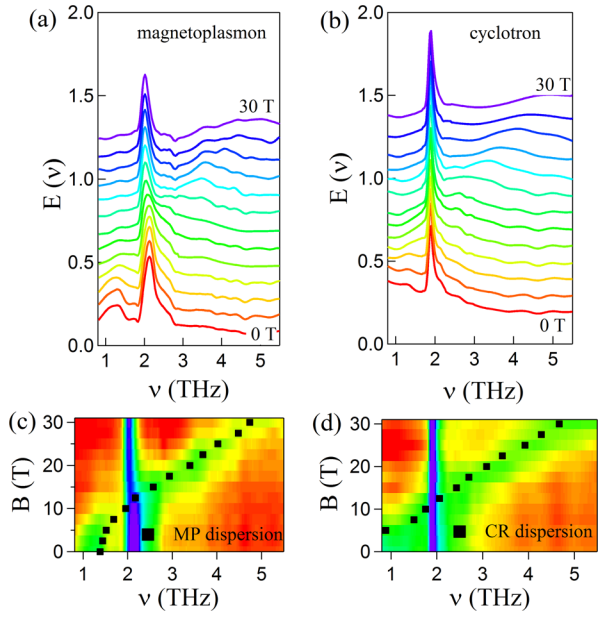

Figure 2. Extinction spectra for Bi_2Se_3 ribbon arrays (W = 8 μm) at 1.6 K for light polarization perpendicular (a) and parallel (b) to ribbons under a magnetic field from 0 to 30 T. Subsequent increasing field spectra are shifted in intensity by a factor +0.1 to better display the behavior of excitations. (c, d) Extinction contour plot obtained from data in (a) and (b), respectively. In this figure, the blue region corresponds to the α-phonon absorption; meanwhile, the green region visually indicates the shift of magnetoplasmon excitation and cyclotron resonance vs B, respectively. Magnetic dispersion curves as extracted from fitting procedures (see text) are shown as black squares.

observed at zero field (see Figure 1c). At higher fields, the phonon mode starts to be less asymmetric and eventually, when the magnetoplasmon is located at high frequency (as expected from eq 1), it presents a symmetric shape. To better show this behavior, a contour plot of the extinction spectra is displayed in Figure 2c, where the magnetoplasmon hardening with B becomes much more evident. In this plot, the blue region corresponds to the phonon absorption, while the green one traces the high-frequency shift of the magnetoplasmon absorption versus B.

In order to extract the bare magnetoplasmon frequency ν_{mp}, we fitted, at each field, the extinction data through a Fano model (see Supporting Information for details), as we made at zero field in Figure 1c. The bare ν_{mp} is shown as black squares in Figure 2c and reported in Figure 3 (blue triangles) versus B. The blue dashed line in the same figure represents a fit to eq 1. The fit, where the only free parameter is the dynamical mass of Dirac carriers m_D^*, provides a value of m_D^* = 0.18 ± 0.01 m_e.

To further estimate the dynamical mass of Dirac carriers, we perform THz measurement for light polarization parallel to the ribbons. These measurements allow us to investigate the Drude single particle response. In this case, the magnetic field causes the localization of the free carriers, transforming the Drude term (centered at zero frequency), into a cyclotron resonance at finite energy (see Figure 2b). This resonance shifts linearly at high frequency with B following eq 2, as can be seen in the extinction contour plot in Figure 2d. A fit to the spectra (see Supporting Information for details) provides the dispersion behavior shown in Figure 3 and also reported in Figure 2d (black squares). In Figure 3, red squares and red dashed line represent experimental cyclotron frequencies and fit to eq 2,

DOI: 10.1021/acsphotonics.5b00036
ACS Photonics 2015, 2, 1231−1235

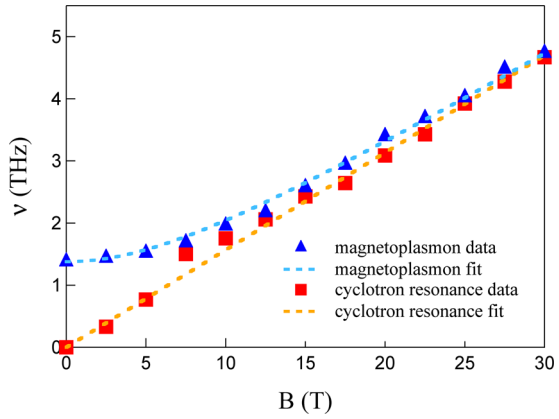

Figure 3. Experimental (blue triangles) magnetoplasmon frequencies vs B, as extracted from a Fano fit of the extinction spectra of Bi_2Se_3 ribbon arrays shown in Figure 2a. The magnetoplasmon dispersion fitted to eq 1 (blue dashed line) provides a dynamical Dirac mass $m_D^* = 0.18 \pm 0.01\ m_e$. Experimental (red squares) cyclotron frequencies as a function of B field, as extracted from fit of the extinction spectra of the unpatterned sample (shown in Figure 2b) and fits to the theoretical behavior of eq 2 (orange dashed line), giving the same value of $m_D^* = 0.18 \pm 0.01\ m_e$.

respectively. The fit provides a Dirac dynamical mass value of $m_D^* = 0.18 \pm 0.01\ m_e$, in perfect agreement with the value extracted from the magnetoplasmonic response (see above). Let us finally observe from Figure 3 that the magnetoplasmon frequency asymptotically approaches the cyclotron frequency as the magnetic field increases, as expected from eq 1.

The Dirac dynamical mass can be compared to the mass of the carriers on the surface of the trivial $(Bi_{0.9}In_{0.1})_2Se_3$ material, where a broad plasmon resonance has been observed at zero field (see Figure 1d). The corresponding THz magnetoplasmon measurements as a function of B are shown in Figure 4a, where the extinction spectra are displayed. Despite the large scattering rate of the massive plasmon characterizing the trivial phase, $\Gamma_{pl}(B = 0, x = 0.1) = 4.95$ THz, the shift of the combined mode is still detectable, as evidenced by the contour plot in Figure 4b. Nevertheless, a fitting procedure as made for the $x = 0$ spectra is not reliable in this case because of the scarce constrast between the magnetoplasmon signal and the background. In order to qualitatively compare the results obtained for Dirac massless and massive carriers, we plot in Figure 4b both the theoretical magnetic-dispersion for massive (blue dotted line) and massless ($m_D^* = 0.18\ m_e$, black dashed line) electrons. Here we assume $m_S^* = 0.12\ m_e$, as reported in literature for the two-dimensional massive carriers due to band bending effects in Bi_2Se_3[21] and $(Bi_{0.9}In_{0.1})_2Se_3$.[19]

From this qualitative comparison one can see that there is a very good agreement between magnetoplasmon dispersion in $(Bi_{0.9}In_{0.1})_2Se_3$ and the mass value of massive surface electrons due to band bending reported in literature.[21] The dispersion for Dirac carriers appears, instead, to be not compatible with the contour plot. This is a further strong indication of the different nature of the two kinds of carriers involved in the magnetoplasmonic excitation and probed in this experiment: massless Dirac electrons in the case of the topological phase with $x = 0$ and massive electrons for the trivial phase with $x = 0.1$.

In summary, in this paper we reported the first experimental observation of magnetoplasmonic resonance in Bi_2Se_3 topological insulator under a strong magnetic field from 0 to 30 T. We probed both the collective and the single-particle response,

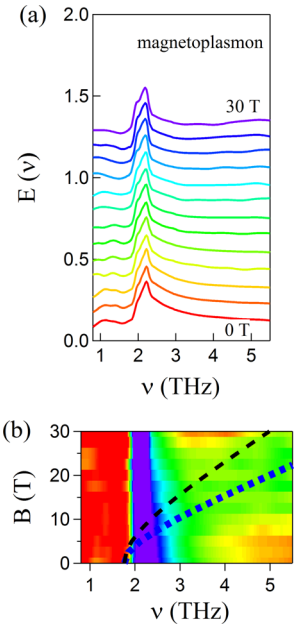

Figure 4. (a) Extinction spectra for $(Bi_{0.9}In_{0.1})_2Se_3$ ribbon arrays ($W = 8\ \mu m$) under a magnetic field from 0 to 30 T. Subsequent increasing field spectra are shifted in intensity by a factor +0.1 to better display the behavior of excitations. (b) Extinction contour plot showing the behavior of magnetoplasmon. The dispersion with $m_S^* = 0.12\ m_e$ (blue dotted line), as in the case of massive surface electrons due to band bending reported in literature,[21] is in very good agreement with data. The magnetic dispersion of Dirac carriers with $m_D^* = 0.18\ m_e$ (black dashed line) is instead not compatible.

comparing experimental magnetic dispersions to theoretical ones and obtaining a dynamical mass $m_D^* = 0.18 \pm 0.01\ m_e$ for Dirac topological carriers. Similar measurements performed on a $(Bi_{0.9}In_{0.1})_2Se_3$ material, which exhibits a trivial topological phase characterized by massive (Schrödinger) electrons with a similar surface carrier density, show a different quantitative behavior, with a magnetoplasmonic dispersion, in agreement with a value $m_S^* = 0.12\ m_e$.

METHODS

Sample Fabrication. High-quality thin films of Bi_2Se_3 were prepared by molecular beam epitaxy using the standard two-step growth method developed at Rutgers University.[10,22] Al_2O_3 ($10 \times 10\ mm^2$) substrates were first cleaned by heating to 750 °C in an oxygen environment to remove organic surface contamination. The substrates were then cooled to 110 °C, and an initial three quintuple layers of Bi_2Se_3 were deposited. This was followed by heating to 220 °C, at which the remainder of the film was deposited to achieve the target thickness. The Se/Bi flux ratio was kept to ~10:1 to minimize Se vacancies. Once the films were cooled, they were removed from the vacuum chamber, vacuum-sealed in plastic bags within 2 min, and then shipped to the University of Rome.

Bi_2Se_3 ribbons were fabricated by electron-beam lithography and subsequent reactive ion etching. The Bi_2Se_3 film was spin-coated with a double layer of electron-sensitive resist polymer poly(methyl methacrylate) (PMMA) to a total thickness of 1.4 μm. Ribbon patterns were then written in the resist by electron-beam lithography. To obtain a lithographic pattern with a realignment precision below 10 nm over a sample area suitable for terahertz spectroscopy of $10 \times 10\ mm^2$, we used an electron

DOI: 10.1021/acsphotonics.5b00036
ACS Photonics 2015, 2, 1231−1235

beam writer equipped with an $x-y$ interferometric stage (Vistec EBPG 5000). The patterned resist served as mask for the removal of Bi_2Se_3 by reactive ion etching at a low microwave power of 45 W to prevent heating of the resist mask. Sulfur hexafluoride (SF_6) was used as the active reagent. The Bi_2Se_3 film was etched at a rate of 20 nm min^{-1}, which was verified by atomic force microscopy after soaking the sample in acetone to remove the PMMA. The in-plane edge quality after reactive ion etching, inspected by atomic force microscopy, closely follows that of the resist polymer mask, that is, with an edge roughness of <20 nm. The vertical profile of the edge forms an angle of ~45° with the substrate plane, because our reactive ion etching process has no preferred etching direction.

■ ASSOCIATED CONTENT

Supporting Information

The Supporting Information is available free of charge on the ACS Publications website at DOI: 10.1021/acsphotonics.5b00036.

Zero-field thin film THz characterization, details on the Fano fit for plasmon−phonon coupling, and methods for the cyclotron resonance analysis (PDF)

■ AUTHOR INFORMATION

Corresponding Author

*E-mail: stefano.lupi@roma1.infn.it.

Notes

The authors declare no competing financial interest.

■ ACKNOWLEDGMENTS

M.B., N.K., and S.O. are supported by Gordon and Betty Moore Foundation and Office of Naval Research (ONR N000141210456). We acknowledge the support of the HFML-RU/FOM, member of the European Magnetic Field Laboratory (EMFL).

■ REFERENCES

(1) Hasan, M. Z.; Kane, C. L. Colloquium: Topological Insulators. *Rev. Mod. Phys.* **2010**, *82*, 3045−3067.

(2) Kane, C. L.; Mele, E. J. Quantum Spin Hall Effect in Graphene. *Phys. Rev. Lett.* **2005**, *95*, 226801.

(3) Moore, J. E. The Birth of Topological Insulators. *Nature* **2010**, *464*, 194−198.

(4) Fu, L.; Collins, G. Computing with Quantum Knots. *Sci. Am.* **2006**, *294*, 56.

(5) Kitaev, A.; Preskill, J. Topological Entanglement Entropy. *Phys. Rev. Lett.* **2006**, *96*, 110404.

(6) Zhang, X.; Wang, J.; Zhang, S.-C. Topological Insulators for High-Performance Terahertz to Infrared Applications. *Phys. Rev. B: Condens. Matter Mater. Phys.* **2010**, *82*, 245107.

(7) Chen, Y. L.; Analytis, J. G.; Chu, J.-H.; Liu, Z. K.; Mo, S.-K.; Qi, X. L.; Zhang, H. J.; Lu, D. H.; Dai, X.; Fang, Z.; Zhang, S. C.; Fisher, I. R.; Hussain, Z.; Shen, Z. Experimental Realization of a Three-Dimensional Topological Insulator, Bi_2Te_3. *Science* **2009**, *325*, 178−181.

(8) di Pietro, P.; Ortolani, M.; Limaj, O.; di Gaspare, A.; Giliberti, V.; Giorgianni, F.; Brahlek, M.; Bansal, N.; Koirala, N.; Oh, S.; Calvani, P.; Lupi, S. Observation of Dirac Plasmons in a Topological Insulator. *Nat. Nanotechnol.* **2013**, *8*, 556.

(9) Autore, M.; D'Apuzzo, F.; di Gaspare, A.; Giliberti, V.; Limaj, O.; Roy, P.; Brahlek, M.; Koirala, N.; Oh, S.; de Abajo, F. J.; Lupi, S. Plasmon-Phonon Interactions in Topological Insulator Microrings. *Adv. Opt. Mater.* **2015**, n/a.

(10) Bansal, N.; Kim, Y. S.; Brahlek, M.; Edrey, E.; Oh, S. Thickness-Independent Transport Channels in Topological Insulator Bi_2Se_3 Thin Films. *Phys. Rev. Lett.* **2012**, *109*, 116804.

(11) Valdès Aguilar, R.; Stier, A. V.; Liu, W.; Bilbro, L. S.; George, D. K.; Bansal, N.; Wu, L.; Cerne, J.; Markelz, A. G.; Oh, S.; Armitage, N. P. Terahertz Response and Colossal Kerr Rotation from the Surface States of the Topological Insulator Bi_2Se_3. *Phys. Rev. Lett.* **2012**, *108*, 087403.

(12) Stauber, T.; Santos, G. G.; Brey, T. Spin-Charge Separation of Plasmonic Excitations in Thin Topological Insulators. *Phys. Rev. B: Condens. Matter Mater. Phys.* **2013**, *88*, 205427.

(13) Ju, L.; Geng, B.; Horng, J.; Girit, C.; Martin, M.; Hao, Z.; Bechtel, H. A.; Liang, X.; Zettl, A.; Shen, Y. R.; Wang, F. Graphene plasmonics for tunable terahertz metamaterials. *Nat. Nanotechnol.* **2011**, *6*, 630−634.

(14) MacDonald, K. F.; Sámson, Z. L.; Stockman, M. I.; Zheludev, N. I. Ultrafast Active Plasmonics. *Nat. Photonics* **2009**, *3*, 55−58.

(15) Armelles, G.; Cebollada, A.; García-Martín, A.; González, M. U. Magnetoplasmonics: Combining Magnetic and Plasmonic Functionalities. *Adv. Opt. Mater.* **2013**, *1*, 10−35.

(16) Alabastri, A.; Toma, A.; Liberale, C.; Chirumamilla, M.; Giugni, A.; Angelis, F. D.; Das, G.; Fabrizio, E. D.; Zaccaria, R. P. Interplay Between Electric and Magnetic Effect in Adiabatic Polaritonic Systems. *Opt. Express* **2013**, *21*, 7538−7548.

(17) Crassee, I.; Orlita, M.; Potemski, M.; Walter, A. L.; Ostler, M.; Seyller, T.; Gaponenko, I.; Chen, J.; Kuzmenko, A. B. Intrinsic Terahertz Plasmons and Magnetoplasmons in Large Scale Monolayer Graphene. *Nano Lett.* **2012**, *12*, 2470−2474.

(18) Yao, X.; Tokman, M.; Belyanin, A. Strong Magneto-Optical Effects Due to Surface States in Three-Dimensional Topological Insulators. *Opt. Express* **2015**, *23*, 795−806.

(19) Brahlek, M.; Bansal, N.; Koirala, N.; Xu, S.-Y.; Neupane, M.; Liu, C.; Hasan, M. Z.; Oh, S. Topological-Metal to Band-Insulator Transition in $(Bi_{1-x}In_x)_2Se_3$ Thin Films. *Phys. Rev. Lett.* **2012**, *109*, 186403.

(20) Wu, L.; Brahlek, M.; Aguilar, R. V.; Stier, A. V.; Morris, C. M.; Lubashevsky, Y.; Bilbro, L. S.; Bansal, N.; Oh, S.; Armitage, N. P. A Sudden Collapse in The Transport Lifetime Across the Topological Phase Transition in $(Bi_{1-x}In_x)_2Se_3$. *Nat. Phys.* **2013**, *9*, 410.

(21) King, P. D. C.; Hatch, R. C.; Bianchi, M.; Ovsyannikov, R.; Lupulescu, C.; Landolt, G.; Slomski, B.; Dil, J. H.; Guan, D.; Mi, J. L.; Rienks, E. D. L.; Fink, J.; Lindblad, A.; Svensson, S.; Bao, S.; Balakrishnan, G.; Iversen, B. B.; Osterwalder, J.; Eberhardt, W.; Baumberger, F.; Hofmann, P. Large Tunable Rashba Spin Splitting of a Two-Dimensional Electron Gas in Bi_2Se_3. *Phys. Rev. Lett.* **2011**, *107*, 096802.

(22) Bansal, N.; Kim, Y. S.; Edrey, E.; Brahlek, M.; Horibe, Y.; Iida, K.; Tanimura, M.; Li, G.-H.; Feng, T.; Lee, H.-D.; Gustafsson, T.; Andrei, E.; Oh, S. Epitaxial Growth of Topological Insulator Bi_2Se_3 Film on Si(111) with Atomically Sharp Interface. *Thin Solid Films* **2011**, *520*, 224−229.

(23) di Pietro, P.; Vitucci, F. M.; Nicoletti, D.; Baldassarre, L.; Calvani, P.; Cava, R.; Hor, Y. S.; Schade, U.; Lupi, S. Optical Conductivity of Bismuth-Based Topological Insulators. *Phys. Rev. B: Condens. Matter Mater. Phys.* **2012**, *86*, 045439.

(24) Giannini, V.; Francescato, Y.; Amrania, H.; Phillips, C. C.; Maier, S. A. Fano Resonances in Nanoscale Plasmonic Systems: A Parameter-Free Modeling Approach. *Nano Lett.* **2011**, *11*, 2835−2840.

(25) Kukushkin, I. V.; Muravev, V. M.; Smet, J. H.; Hauser, M.; Dietsche, W.; von Klitzing, K. Collective Excitations in Two-Dimensional Electron Stripes: Transport and Optical Detection of Resonant Microwave Absorption. *Phys. Rev. B: Condens. Matter Mater. Phys.* **2006**, *73*, 113310.

(26) Novoselov, K. S.; Geim, A. K.; Morozov, S. V.; Jiang, D.; Katsnelson, M. I.; Grigorieva, I. V.; Dubonos, S. V.; Firsov, A. A. Two-Dimensional Gas of Massless Dirac Fermions in Graphene. *Nature* **2005**, *438*, 197−200.

DOI: 10.1021/acsphotonics.5b00036
ACS Photonics 2015, 2, 1231−1235